



Extraction of gadolinium on Cu electrode from LiCl-KCl melts by formation of Cu-Gd alloys

Yingcai Wang^{1,2,3} · Yuhui Liu^{2,3} · Mei Li¹ · Wei Han¹ · Yibao Liu^{2,3} · Yunhai Liu²

Received: 26 July 2018 / Revised: 13 September 2018 / Accepted: 7 October 2018 / Published online: 18 October 2018
© Springer-Verlag GmbH Germany, part of Springer Nature 2018

Abstract

Electrochemical behavior of gadolinium was studied on W and Cu electrodes in LiCl-KCl melts 823 K via cyclic voltammetry, square wave voltammetry, and open circuit chronopotentiometry. The reduction of Gd(III) ions was found to be through a one-step process: $\text{Gd(III)} + 3e^- = \text{Gd(0)}$. The equilibrium potential of the Gd(III)/Gd(0) redox couple was measured via open circuit chronopotentiometry in the temperature range of 773–893 K, with subsequent calculation of the apparent standard potential, $E_{\text{Gd(III)/Gd(0)}}^{*0}$, and the apparent Gibbs free energy of formation for GdCl_3 , $\Delta G_f^{*0}(\text{GdCl}_3)$. Three reduction peaks, corresponding to the formation of Gd_xCu_y intermetallic compounds, were detected from cyclic voltammogram and square wave voltammogram obtained by co-reduction of Gd(III) and Cu(II) ions or electrodeposition of Gd(III) on Cu electrode. Potentiostatic/galvanostatic electrolysis was performed on Cu electrode with different electrolytic conditions. The results indicate that the Cu-Gd alloys are comprised of CuGd, Cu_2Gd , and Cu_6Gd phases. The morphology and micro-zone chemical analysis of the deposits were characterized by scanning electron microscopy (SEM) equipped with energy dispersive spectrometry (EDS). The highest extraction efficiency of metallic Gd could reach about 99.60% at -2.20 V for 12 h at 823 K. Therefore, employing electrochemical deposition of Gd(III) on reactive Cu electrode to extract Gd is feasible.

Keywords Electrochemical extraction · Extraction efficiency · Electrolysis · LiCl-KCl melts · Cu-Gd alloy

Introduction

Molten salt-based high-temperature chemical treatment technology has been considered to be the promising techniques for nuclear-related research and development, especially in the field of dry reprocessing of spent fuel. Reasonable utilization and full recovery of spent nuclear fuel are key issues for nuclear power plant. To reduce the output and long-lived

radiotoxicity of spent fuel and high-level waste (HLW), partitioning and transmutation (P&T) strategies have become a potential option for the advanced fuel cycle and an alternative for complementary waste management [1, 2]. P&T concepts are have been extensively researched, because they made it possible to reduce the volume and the long-term radiotoxicity of nuclear fuels. P&T requires recycling of the radiotoxic higher lanthanides and actinides. For the extraction and separation of lanthanides and actinides, various separation methods (based on electrochemical theory) are currently under development, for example, electrorefining and electrolysis in melts. The accuracy of experimental data is significant for extraction and separation of lanthanides and actinides. However, the separation of rare earth (RE) is difficult due to their similar chemical properties. For the reason, a good knowledge of the basic chemical and electrochemical behaviors of RE elements in the proposed separation media is very significant to determine the available separation methods. In reactor physics, nuclear poison (rare earth elements account for 25%) has a large capacity for absorbing neutrons in a nuclear reaction [3]. The effect may be negative in some reactor applications because the fission chain reaction may be

✉ Wei Han
weihan@hrbeu.edu.cn

✉ Yunhai Liu
walton_liu@163.com

¹ Key Laboratory of Superlight Materials and Surface Technology, Ministry of Education, College of Materials Science and Chemical Engineering, Harbin Engineering University, Harbin 150001, China

² Engineering Research Center of Nuclear Technology Application, Ministry of Education, East China University of Technology, Nanchang 330013, China

³ School of Nuclear Science and Engineering, East China University of Technology, Nanchang 330013, China

prevented and disrupted, thereby affecting normal reactions. In conclusion, most of the rare earth elements as much as possible should be removed. However, the extraction and separation of rare earth has been widely studied on active electrode in melts.

In melts, the current effective methods to separate and extract RE elements is using active electrode (Cu, Ni, Mg, Al, Bi, Co, and Zn) as the cathode to the formation of intermetallic compounds by making their deposition potential move to a more positive direction [4–13], such as Al [14–25], Cu [26–33], Ni [30, 34–40], and Mg [41, 42]. Castrillejo et al. have discussed electrochemical mechanism of Pr [14], Dy [15], Gd [16], Er [17], Ho [18], Eu [19], Lu [20], Tm [21], Yb [22], Sm [23], and Tb [24] in LiCl-KCl melts on reactive Al electrode. The electrochemical behavior of Pr [34], Dy [35] and Nd [36] have been reported by Yasuda et al., and Konishi et al. and Iida et al. have researched electrochemical deposition of Tb [38], Yb [39], and Sm [40] on Ni electrode. The extraction and separation of Yb [32] and Ho [33] have been discussed by Mei Li and Zhuyao Li et al., and intermetallic compounds are obtained. We previously studied the extraction of metallic Er on Cu electrode with high extraction efficiency (98.92%).

In this paper, electrochemical mechanism and thermodynamic data of gadolinium as one of lanthanides is discussed in LiCl-KCl melts on W and Cu electrode. The corresponding Cu-RE intermetallic compounds were obtained on Cu electrode. By employing electrolytic deposition of metallic Gd on reactive Cu electrode to extract Gd element, the extraction efficiency of rare earth is calculated. The focus of the paper is that the electrochemical process and high extraction efficiency of metallic Gd in LiCl-KCl melts.

Experimental preparation and equipment

LiCl (99.9%)-KCl (99.9%) molten salt system (weight ratio = 50 g/50 g) was dried under argon for over 24 h at 473 K to remove water before being used. Gd(III) and Cu(II) ions were added into LiCl-KCl melts in the form of CuCl_2 (99.9%) and GdCl_3 (99.9%) without water, respectively. All experiments were operated in argon atmosphere which was maintained to avoid contact with O_2 and H_2O .

Cyclic voltammetry, square wave voltammetry, open circuit chronopotentiometry and potentiostatic/galvanostatic electrolysis tests controlled with the Nova 1.10 software were performed using an Autolab PGSTAT 302N. The electrochemical measurements with three-electrode device were performed in a quartz crucible. The working electrode was a tungsten wire ($\varphi = 1$ mm), a copper wire ($\varphi = 2$ mm), and a copper piece ($S = 2$ mm \times 2 mm). The lower extreme of the working electrode was polished completely with SiC sandpaper and then cleaned using ultrasonic cleaning equipment to

remove oxidation film and impurities of electrode surface. The counter electrode was a spectral pure graphite rod ($\varphi = 6$ mm). Ag/AgCl couple was used as reference electrode, which consisted of AgCl (1.0 wt.%) in LiCl-KCl melts.

Potentiostatic/galvanostatic electrolysis was carried out to extract Gd element on Cu electrode. Then the samples were successively polished with 3000# SiC sandpaper. The analysis and characterization of the samples were via X-ray diffraction (XRD) (Rigaku D/max-TTR-III diffractometer) using Cu-K α radiation at 40 kV and 150 mA. The microstructure and microzone chemical of Cu-Gd alloys were analyzed by scanning electron microscopy (SEM) equipped with energy dispersive spectrometry (EDS) (JSM-6480A; JEOL Co., Ltd.).

Results and discussion

Electrochemical process of Gd(III) on W electrode

The electrochemical mechanism of gadolinium chlorides in LiCl-KCl melts was researched by several kinds of electrochemical methods, such as cyclic voltammetry, square wave voltammetry, and open circuit chronopotentiometry.

Figure 1 shows the cyclic voltammograms obtained on tungsten electrode in the absence and in the presence of GdCl_3 . The dashed curve of purified blank salt has no additional reaction signal within the examined electrochemical window except the currents corresponding to the reduction/oxidation of Li. The solid line clearly shows a new pair of redox peak after the addition of GdCl_3 . The signals A/A', detected at about -2.04 V/ -1.83 V (vs Ag/AgCl), are ascribed to characteristic of formation of a new solid phase (pure Gd).

Figure 2a exhibited a series of cyclic voltammograms obtained on W electrode with different scan rates. The variation

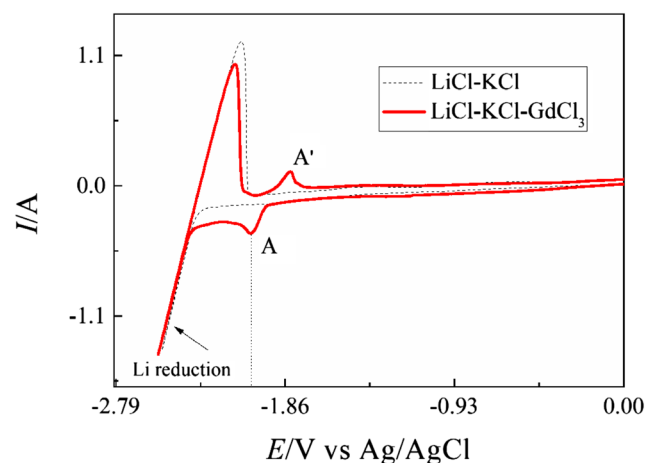


Fig. 1 Figure 1 shows the cyclic voltammograms obtained on tungsten electrode in the absence and in the presence of GdCl_3 . Temperature: 823 K; scan rate: 0.1 V s^{-1}

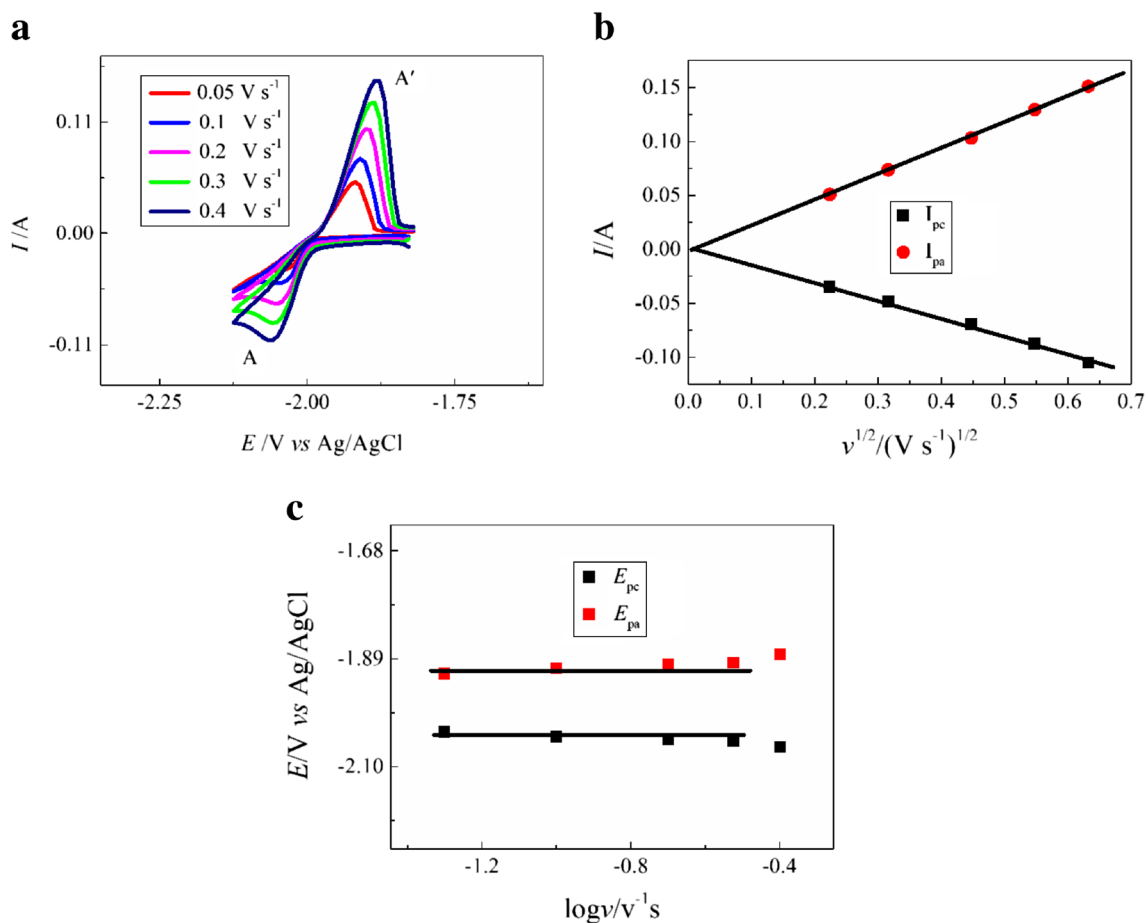


Fig. 2 **a** Exhibited a series of cyclic voltammograms obtained on W electrode with different scan rates; **b** variation of the cathodic and anodic peak currents with the square root of the scan rates; **c** variation

of the cathodic and anodic peak potentials with the logarithm of the scan rates. Temperature: 823 K

of peak currents and potentials of voltammogram are recorded by the change of scan rate.

The linear relation of the square root of the scan rate and the peak current was observed in Fig. 2b. On the basis of linear sweep voltammetry [43], the electrode process is controlled by the rate of mass transfer when scan rate reaches 0.3 V s^{-1} . As the scan rate gets larger, the electron transfer rate becomes significantly lower than that of mass transport. Figure 2c shows that the reversibility of the system was discussed by researching the relation of the peak potential and the scan rate. The peak potential, E_p , is basic constant with a low scan rate, whereas, for the higher scan rates, the anodic and cathodic peak potentials change slightly towards more positive and negative, respectively. These results indicate that the reduction of Gd(III) ions on W electrode is reversible at low scan rates.

Only a peak A detected within the electrochemical window indicates that deposition of gadolinium is a step three-electron process [44]. The width of the half-peak, $W_{1/2}$, is related to the electrons transfer numbers as follows [45, 46]:

$$W_{1/2} = 3.52RT/nF \tag{1}$$

where R is the ideal gas constant ($\text{J mol}^{-1} \text{ K}^{-1}$); F is the Faraday constant (C mol^{-1}); T is the temperature (K) and n is the number of exchanged electrons.

Figure 3 displays the square wave voltammograms (SWVs) obtained on W electrode with different frequencies in LiCl-KCl-GdCl₃ melts. The validity of Eq. (1) was proved by plotting the peak current vs the square root of the frequency [46, 47]. The straight line going through the origin (see inset in Fig. 3) demonstrates that Eq. (1) can be used to calculate the number of electrons in the frequency range discussed [46]. According to the half-height width of peaks A, the transfer electron numbers are 2.79, 2.86, 2.84, and 2.88 (average value: 2.84), respectively, which suggests that the reduction process of Gd(III) proceeds as a one-step process involving three electrons.

The calculation of apparent Gibbs free energy of formation for GdCl₃

Open circuit chronopotentiometry is an electrochemical method by researching the deposition and dissolution of alloys. The

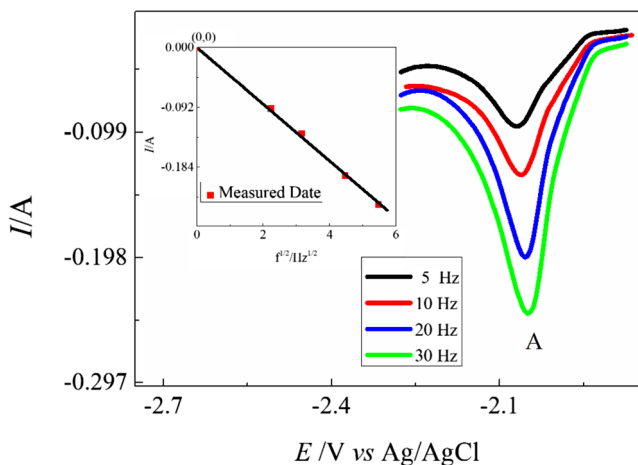


Fig. 3 Square-wave voltammograms at different frequencies obtained in LiCl-KCl-1.48 wt.% GdCl₃ melts on W electrode; Inset: the linear relationship of I versus $f^{1/2}$ for square-wave voltammograms. Temperature: 823 K

open potential (E) vs time (T) was detected in the absence of current. Figure 4 expresses open circuit potential curves obtained at different temperatures in LiCl-KCl-GdCl₃ (1.48 wt.%) melts on W electrode by electrodeposition at -2.50 V vs Ag/AgCl at different deposition times. A series of stable plateau were detected in Fig. 4, measuring the corresponding equilibrium potential. The measured potentials for the Gd(III)/Gd(0) are determined by the Nernst equation:

$$E_{\text{Gd(III)/Gd(0)}}^{\text{eq}}(\text{V vs Ag/AgCl}) = E_{\text{Gd(III)/Gd(0)}}^0 + \frac{RT}{3F} \ln \frac{a_{\text{Gd(III)}}}{a_{\text{Gd(0)}}} \quad (2)$$

where $a_{\text{Gd(III)}}$ and $a_{\text{Gd(0)}}$ are the activity of Gd(III) ions and metal Gd, respectively, while $E_{\text{Gd(III)/Gd(0)}}^{\text{eq}}$ is the standard potential at a hypothetical liquid reference state of unit mole

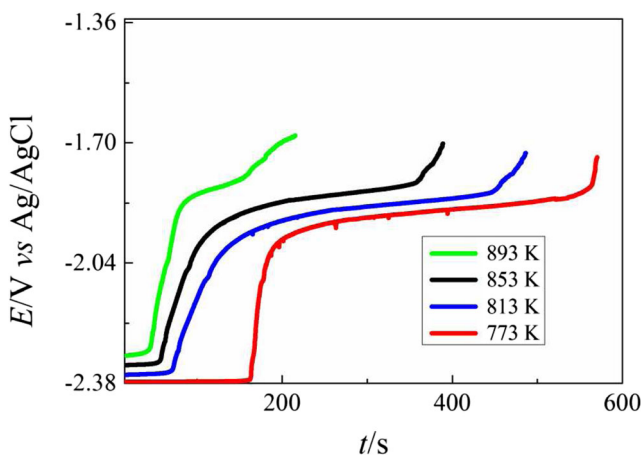


Fig. 4 Open circuit potential curves obtained at different temperatures in LiCl-KCl-GdCl₃ (1.48 wt.%) melts on W electrode by electrodeposition at -2.50 V vs Ag/AgCl at different deposition times

fraction and unit activity. The apparent standard potential, $E_{\text{Gd(III)/Gd(0)}}^{\ast 0}$, for the Gd(III)/Gd(0) redox couple is defined as:

$$E_{\text{Gd(III)/Gd(0)}}^{\ast 0} = E_{\text{Gd(III)/Gd(0)}}^0 + \frac{RT}{3F} \ln \gamma_{\text{Gd(III)}} \quad (3)$$

where $\gamma_{\text{Gd(III)}} = a_{\text{Gd(III)}}/X_{\text{Gd(III)}}$, $\gamma_{\text{Gd(III)}}$ is the activity coefficient of Gd(III), and $X_{\text{Gd(III)}}$ is the molar fraction of Gd(III) in melts. Equation (2) and Eq. (3) can be expressed as:

$$E_{\text{Gd(III)/Gd(0)}}^{\text{eq}}(\text{V vs Ag/AgCl}) = E_{\text{Gd(III)/Gd(0)}}^{\text{eq}} + \frac{RT}{3F} \ln X_{\text{Gd(III)}} \quad (4)$$

The potential values with respect to the Cl₂/Cl⁻ system were obtained by the following equations.

$$E_{\text{Ag/AgCl}}(\text{V vs Cl}_2/\text{Cl}^-) = E_{\text{AgCl}}^0 + \frac{RT}{1F} \ln X_{\text{AgCl}} \quad (5)$$

$$E_{\text{Ag/AgCl}}(\text{V vs Cl}_2/\text{Cl}^-) = -1.0910 - 1.857 \times 10^{-4} T(\text{K}) \quad (6)$$

$$E_{\text{Gd(III)/Gd(0)}}^{\ast 0}(\text{V vs Cl}_2/\text{Cl}^-) = E_{\text{Gd(III)/Gd(0)}}^{\text{eq}}(\text{V vs Ag/AgCl}) + E_{\text{Ag/AgCl}}(\text{V vs Cl}_2/\text{Cl}^-) - \frac{RT}{3F} \ln X_{\text{Gd(III)}} \quad (7)$$

Table 1 shows that the apparent potential values with different temperatures are exhibited. According to Table 1, the linear relationship of apparent standard potential changing with temperature can be defined as:

$$E_{\text{Gd(III)/Gd(0)}}^{\ast 0}(\text{V vs Cl}_2/\text{Cl}^-) = -3.154 + 3.120 \times 10^{-4} T(\text{K}) \quad (8)$$

Therefore, the apparent standard Gibbs free energy of the formation for GdCl₃ can be calculated by the following expression:

$$G_f^{\ast 0}(\text{GdCl}_3) = -3FE_{\text{Gd(III)/Gd(0)}}^{\ast 0} \quad (9)$$

Table 2 shows the results of the apparent Gibbs free energy of the formation for GdCl₃. The variation of apparent Gibbs free energy of formation for GdCl₃ with temperature is exhibited in Fig. 5.

$$G_f^{\ast 0}(\text{GdCl}_3) = -1007.304 + 0.17949T \quad (10)$$

The apparent Gibbs free energy is also a function of temperature:

$$\Delta G_f^{\ast 0}(\text{GdCl}_3) = \Delta H_f^{\ast 0}(\text{GdCl}_3) - T\Delta S_f^{\ast 0}(\text{GdCl}_3) \quad (11)$$

Table 1 The apparent potential values with different temperatures are exhibited

T/K	$E_{\text{Gd(III)/Gd(0)}}^{\text{app}}/\text{V}$ vs Ag/AgCl	$E_{\text{Gd(III)/Gd(0)}}^{\text{app}}/\text{V}$ vs Ag/AgCl	$E_{\text{Gd(III)/Gd(0)}}^{\text{app}}/\text{V}$ vs Cl ₂ /Cl ⁻		
				La [44]	Er [31]
773	-1.894	-1.765	-3.00	-	-2.914
813	-1.869	-1.734	-2.98	-3.040	-
853	-1.843	-1.701	-2.95	-	-
893	-1.818	-1.669	-2.93	-	-

Therefore, the apparent standard enthalpy ($\Delta H_f^{\text{app}}(\text{GdCl}_3)$) and entropy ($T\Delta S_f^{\text{app}}(\text{GdCl}_3)$) of formation for GdCl₃ are -1007.304 kJ mol⁻¹ and -179.49 J mol⁻¹ K⁻¹, respectively, which were similar to the research results for LaCl₃ obtained by Castrillejo et al. (-1045.3 kJ mol⁻¹ and -185.6 J mol⁻¹ K⁻¹) [48] and Fusselman et al. (-1053.9 kJ mol⁻¹ and -197.9 J mol⁻¹ K⁻¹) [49].

On the basis of the difference value between the apparent Gibbs free energies of formation for GdCl₃ ($G_f^{\text{app}}(\text{GdCl}_3)$), the activity coefficient of Gd(III) was calculated from and the Gibbs free energies of formation for GdCl₃ ($G_f^0(\text{GdCl}_3, \text{SC})$) in LiCl-KCl melts as follows:

$$2.303RT \log \gamma_{\text{GdCl}_3} = \Delta G_f^{\text{app}}(\text{GdCl}_3) - \Delta G_f^0(\text{GdCl}_3, \text{SC}) \quad (12)$$

where $\Delta G_f^0(\text{SC})$ is the Gibbs free energy of formation for GdCl₃ from the reaction of the pure compounds in the supercooled state. The Gibbs free energies of formation for GdCl₃ in the supercooled state are summarized in Table 3. The order of magnitude of the calculated activity coefficients is approximately 10⁻⁴. Compared with the results obtained by Bagri et al. [50] and Zhou et al. [51], order of magnitudes of the results were all about 10⁻⁴.

Co-reduction process of CuCl₂ and GdCl₃

Figure 6 shows that cyclic voltammograms obtained on W electrode in LiCl-KCl-GdCl₃ (1.46 wt.%) - CuCl₂ (0.98 wt.%) melts. To determine the accuracy of peak potential, the cyclic voltammetry with different termination potentials (-2.1 V, -2.0 V, and -1.9 V) were operated. Five pairs of reduction-

oxidation peaks A/A', I/I', II/II', III/III', and B/B' were detected within the range of the electrochemical window. The reduction potential starts to increase from about -0.15 V and peaking at about -0.24 V (signal B), which is caused by the deposition of Cu(I) to Cu [33, 52]. Therefore, the peaks I', II', and III' at about -1.99 V, -1.89 V, and -1.80 V between the deposition potential of Cu and Gd should be corresponded to the deposition of Cu-Gd intermetallic compounds, which is formed through underpotential deposition of Gd on Cu electrode. Therefore, the deposition potential value of Gd(III) on Cu electrode is more positive than one of Gd(III) on W electrode. The formation process of Cu-Gd intermetallic compounds can be expressed by the following three steps: (1) xCu(II) + xe⁻ ⇌ xCu(I); (2) xCu(I) + xe⁻ ⇌ xCu(0), yGd(III) + 3ye⁻ ⇌ yGd; (3) yGd + xCu ⇌ Gd_yCu_x. The whole process of the formation of Cu-Gd alloy can be expressed as follow:

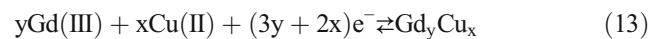


Figure 7a displays square wave voltammograms obtained in LiCl-KCl-GdCl₃ (1.46 wt.%) - CuCl₂ (0.98 wt.%) melts on W electrode at 823 K. It exhibits five obvious peaks with the potentials of -2.05 V, -1.98 V, -1.88 V, and -1.79 V, which correspond to the formation of pure Gd metal, three different Cu-Gd alloys and the deposition of Cu metal, respectively. The height of peak A decreases obviously addition of 1.46 wt.% GdCl₃ on account of the formation of intermetallics. A very thin layer of Cu-Gd alloy was prepared by cathodic deposition on W electrode at deposition potential of -2.5 V in LiCl-KCl-GdCl₃ (1.46 wt.%) - CuCl₂ (0.98 wt.%) melts. Similarly, four electrochemical platforms at potential -1.91 V, -1.78 V, -1.70 V, and -1.56 V were detected in

Table 2 Comparison of thermodynamic data for GdCl₃ obtained in the LiCl-KCl melts with different temperatures

Temperature/ K	$G_f^{\text{app}}(\text{GdCl}_3)/\text{kJ mol}^{-1}$	$G_f^0(\text{GdCl}_3, \text{SC})/\text{kJ mol}^{-1}$ [45]	$\log \gamma_{\text{GdCl}_3}$	γ_{GdCl_3}
773	-868.500	-816.191	-3.534	2.92×10^{-4}
813	-861.552	-806.555	-3.533	2.93×10^{-4}
853	-854.025	-796.969	-3.493	3.21×10^{-4}
893	-847.007	-788.097	-3.445	3.59×10^{-4}

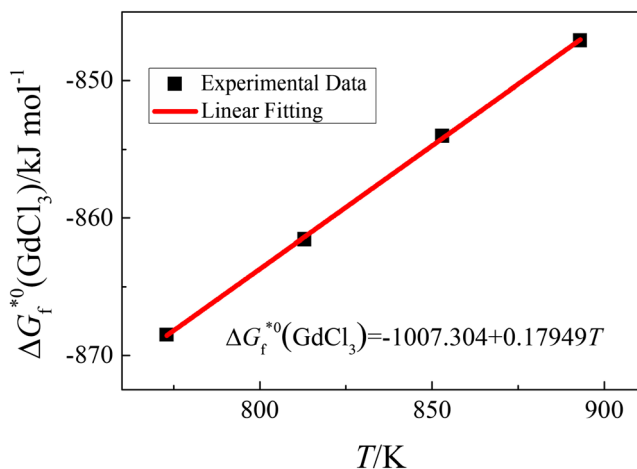


Fig. 5 Variation of the Gibbs free energy of the formation for GdCl_3 with temperature in melts

Fig. 7b, respectively. Since Gd metal deposited on Cu, and diffuses into the Cu electrode, the potential value of Cu-Gd intermetallic compound gradually shifts to more positive. The possible platform equilibrium reaction involves two steps described as follows: (1) $x\text{Gd}(0) - xe^- = x\text{Gd}(\text{III})$; (2) $z\text{Cu}_x\text{Gd}_y - 3(zy-xm)e^- = x\text{Cu}_z\text{Gd}_m + (zy-xm)\text{Gd}(\text{III})$ (equilibrium reaction of platform I, II, and III).

Electrochemical behavior of GdCl_3 on Cu electrode

To further explore the formation of Cu-Gd intermetallic compounds, we researched the cyclic voltammograms obtained on Cu electrode at 823 K in LiCl-KCl-GdCl_3 (1.48 wt.%). In Fig. 8, five pairs of peaks A/A', I/I', III/III', and B were obtained, which corresponds to the deposition/dissolution of Gd metal, three different Cu-Gd intermetallic compounds and Cu metal, respectively. Three pairs of reduction/oxidation peaks, I/I', II/II', and III/III' at $-1.98\text{ V}/-1.73\text{ V}$, $-1.91\text{ V}/-1.51\text{ V}$, and $-1.79\text{ V}/-1.41\text{ V}$, are clearly observed. As the scan rate increases, the peak current value is getting larger.

Table 3 The extraction efficiency of LiCl-KCl-GdCl_3 (1.48 wt.%) melts obtained during potentiostatic electrolysis at -2.20 V (vs Ag/AgCl) on Cu electrode

Electrolytic time (h)	The concentration of GdCl_3 in melts (wt.%)	Extraction efficiency (%)
0	0.99	0
1	0.90	11.11
2	0.78	21.21
4	0.60	39.39
6	0.43	56.57
8	0.26	72.72
10	0.13	86.86
12	0.004	99.60

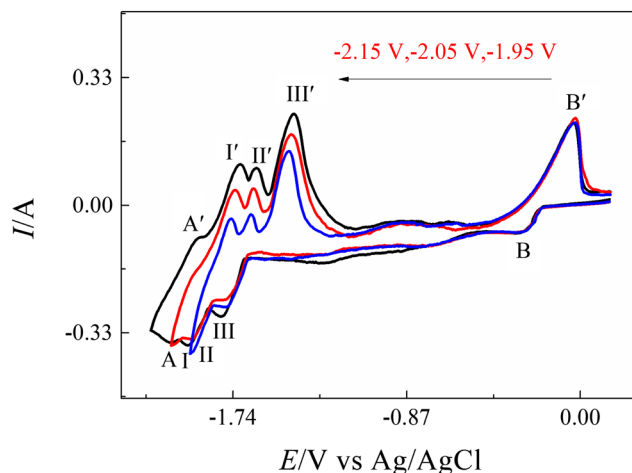


Fig. 6 Cyclic voltammograms curves obtained in LiCl-KCl-GdCl_3 (1.46 wt.%) - CuCl_2 (0.98 wt.%) melts. Work electrode: tungsten; temperature: 823 K

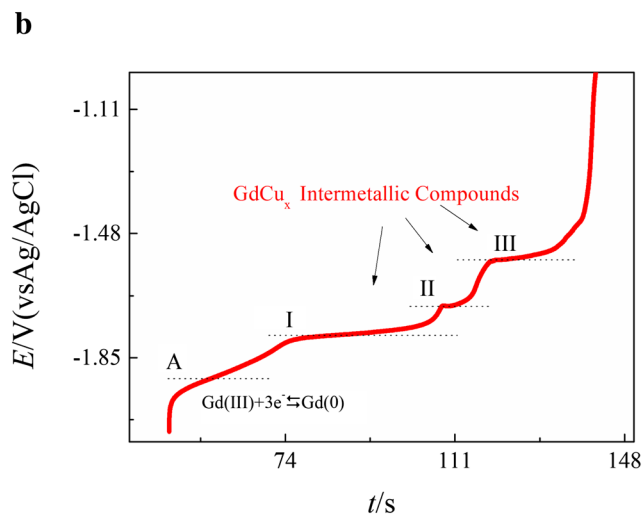
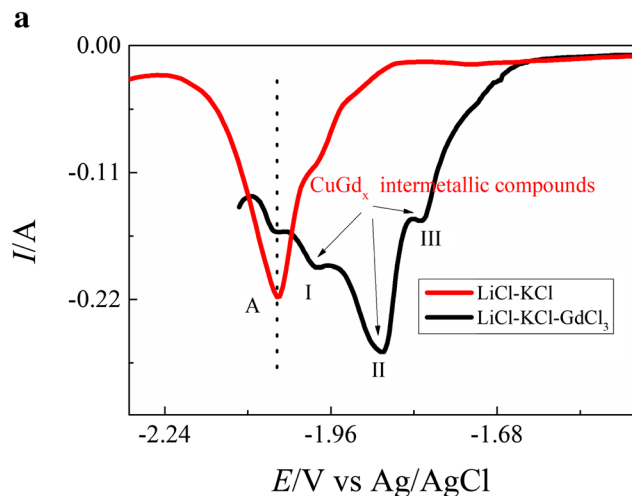


Fig. 7 **a** Square wave voltammetry; **b** Open circuit chronopotentiometry curves obtained in LiCl-KCl-GdCl_3 (1.46 wt.%) - CuCl_2 (0.98 wt.%) melts on W electrode. Temperature: 823 K; electrodeposition time: 30 s

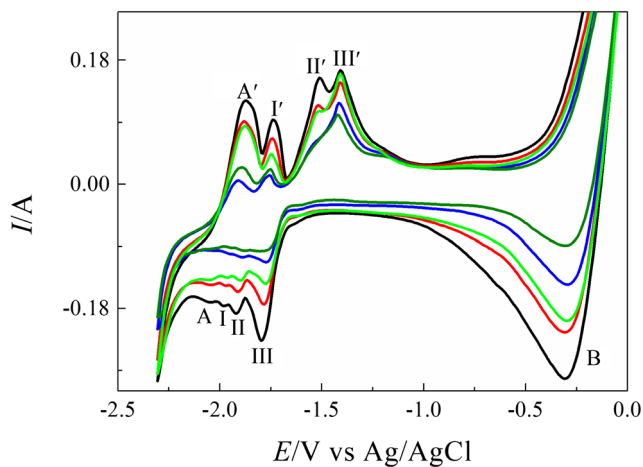


Fig. 8 Cyclic voltammograms obtained on Cu electrode in LiCl-KCl-GdCl₃ (1.48 wt.%) at different scan rates. Work electrode: tungsten; temperature: 823 K

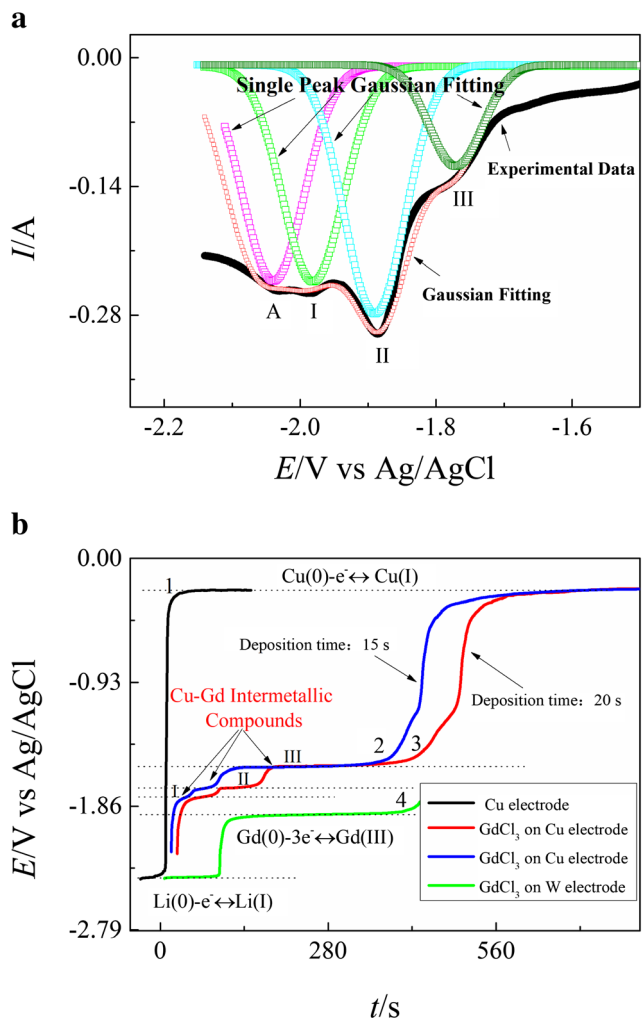


Fig. 9 a Square wave voltammetry in LiCl-KCl-GdCl₃ (1.48 wt.%) melts; b Open circuit chronopotentiometry with different molten salt systems. Work electrode: tungsten; temperature: 823 K; frequency: 25 Hz

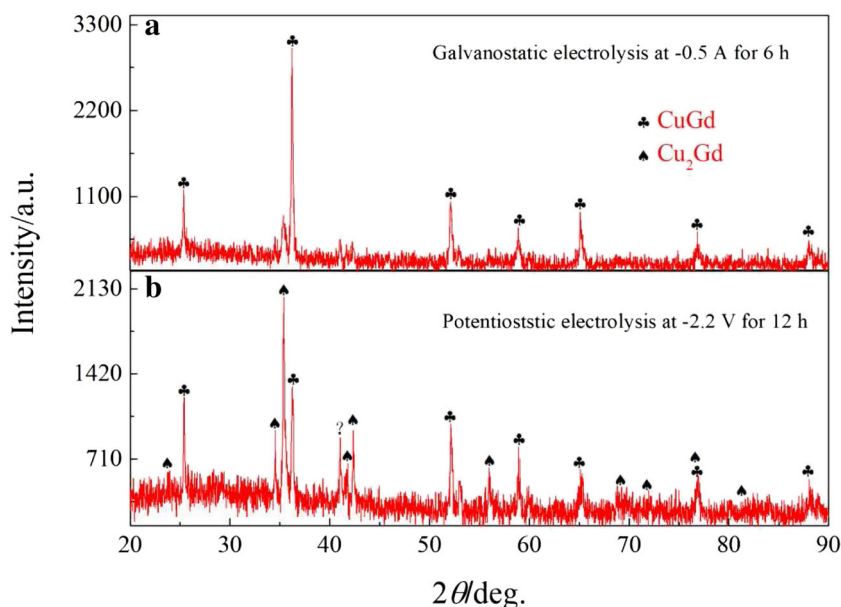
Figure 9a shows square wave voltammetry obtained in LiCl-KCl-GdCl₃ (1.46 wt.%) melts on Cu electrode. In order to detect the peak clearly, Gaussian fitting was adopted in Fig. 9a. It exhibits four obvious peaks with the potentials of -2.04 V, -1.99 V, -1.89 V, and -1.78 V, which correspond to the formation of pure Gd metal, three different Cu-Gd alloys and the deposition of Cu metal, respectively. The potential values of intermetallic compounds on Cu electrode were similar with the one on W electrode. Figure 9b exhibits open circuit chronopotentiometry with different molten salt systems. Curve 4 corresponds to the open circuit chronopotentiometry obtained in LiCl-KCl-GdCl₃ melts on W electrode after potentiostatic electrolysis at -2.5 V for 30 s. The potential stays at about -2.38 V (curve 1), which is by reason of the deposits of Li metal on W electrode. Therefore, the equilibrium potential of Li(I)/Li(0) in LiCl-KCl melts is about -2.38 V at 823 K. However, the equilibrium potential of Gd(III)/Gd is at about -1.92 V. Curve (2 and 3) demonstrates the open circuit chronopotentiogram are performed in LiCl-KCl-GdCl₃ melts with deposition potential -2.30 V for 20 s. In curve 2 and 3, the plateau potential of I, II, and III become more positive. This phenomenon is attributed to the formation of Cu-Gd alloys. Curve 4 is associated with the open circuit chronopotentiogram conducted in LiCl-KCl melts on Cu electrode. Only a plateau (Cu - e⁻ ⇌ Cu(I)) was detected.

Potentiostatic/galvanostatic electrolysis and characterization of the Cu-Gd alloys

Electrochemical extraction of Gd element was carried out by galvanostatic/potentiostatic electrolysis on Cu electrode. The preparation of Cu-Gd alloys has been performed via galvanostatic/potentiostatic electrolysis. Figure 10a shows the XRD patterns of the deposits obtained on Cu electrode in LiCl-KCl melts containing 1.48 wt.% GdCl₃ after galvanostatic electrolysis at -0.5 A for 6 h. The Cu-Gd alloy is composed of Cu₂Gd phase as shown XRD patterns of Fig. 10a. When the electrolytic condition was changed to potentiostatic electrolysis, Cu-Gd alloy contains Cu₂Gd and CuGd phases by the analysis of XRD. According to the analysis of SEM/EDS below, the plating consists of two layers (Cu₂Gd and CuGd intermetallic compounds).

Microstructure analysis of the elements was applied to research the distribution of Gd element in Cu-Gd alloys. Figure 11 exhibits a set of SEM micrograph of a cross section of Cu-Gd alloys obtained via galvanostatic electrolysis at -0.5 A for 2 h. From these images, Cu-Gd alloys were clearly distinguished by two phases (dark and bright parts). The bright part is known as the Cu-Gd phase, and the dark part is corresponding to Cu phase. Many different lightspots randomly distribute on the surface in SEM images. The dark and bright parts are Cu substrate and Cu-Gd intermetallics, respectively, which are displayed via EDS mapping analysis. The

Fig. 10 The XRD patterns of the deposits obtained on Cu electrode in LiCl-KCl melts containing 1.48 wt.% GdCl₃ after galvanostatic electrolysis at -0.5 A for 6 h and potentiostatic electrolysis -2.20 V for 12 h, respectively



conclusions of EDS quantitative analysis of the points labeled A district mean that the clad layer is composed of Cu and Gd elements. For the point A in Fig. 11a, the atom percentage ratio Cu/Gd is about 85.77/14.23 (6.03/1). Combined with the XRD result, we think the Cu-Gd phase is CuGd compound. Figure 12 shows a group of SEM/EDS mapping analysis of the Cu-Gd alloy by galvanostatic electrolysis at -0.5 A for 6 h. Because of the extended electrolysis time, the coating is thicker than that in Fig. 11a. For the point A in Fig. 12a, the atom percentage ratio Cu/Gd is about 49.67/50.33 (0.99/1); therefore, Cu-Gd phase is Cu₂Gd intermetallic compound.

In order to completely extract Gd element, potentiostatic electrolysis at -2.20 V for 12 h is performed in LiCl-KCl-GdCl₃ (1.48 wt.%) melts on Cu electrode. The two coating can be clearly observed, and the EDS results of the red frame labeled A and B district from Fig. 13a mean that the layer included Cu and Gd, with the Cu/Gd atomic ratio of about 67.60/32.40 (2.09/1) and 45.74/54.26 (1.05/1), respectively. Therefore, the phase is composed of Cu₂Gd and CuGd phases. Table 3 shows the ICP/AES analysis of supernatant in melts obtained at different electrolytic time by potentiostatic electrolysis. The extraction efficiency for gadolinium is about

Fig. 11 SEM micrograph and EDS analysis of a cross section of Cu electrode in LiCl-KCl-GdCl₃ (1.48 wt.%) melts by galvanostatic electrolysis at -0.5 A for 2 h. Temperature: 823 K

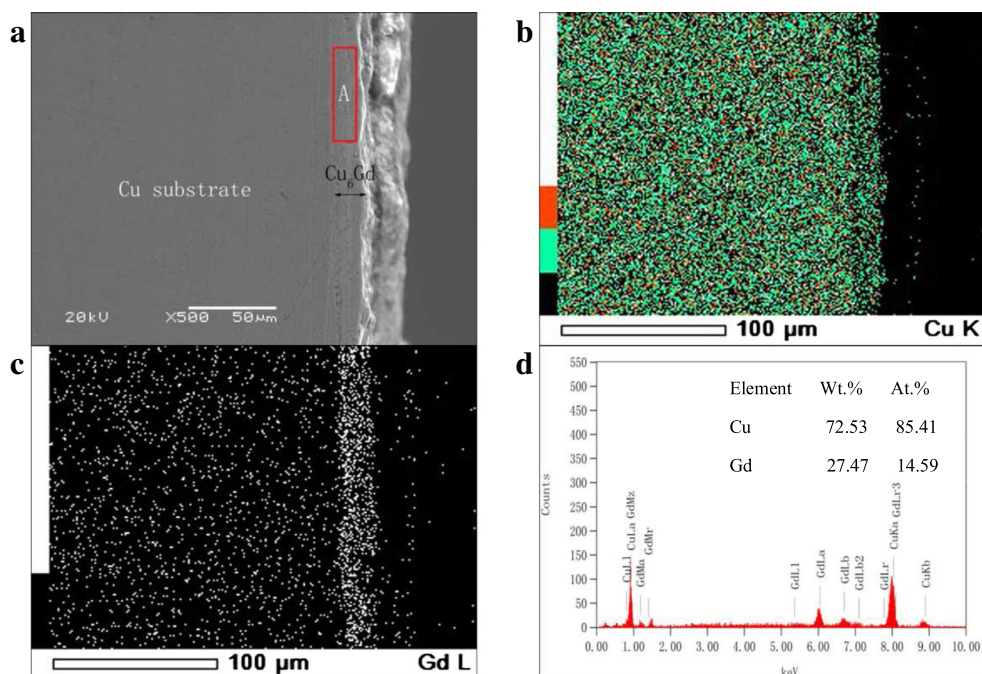


Fig. 12 SEM micrograph and EDS analysis of a cross section of Cu electrode in LiCl-KCl-GdCl₃ (1.48 wt.%) melts by galvanostatic electrolysis – 0.5 A for 6 h. Temperature: 823 K

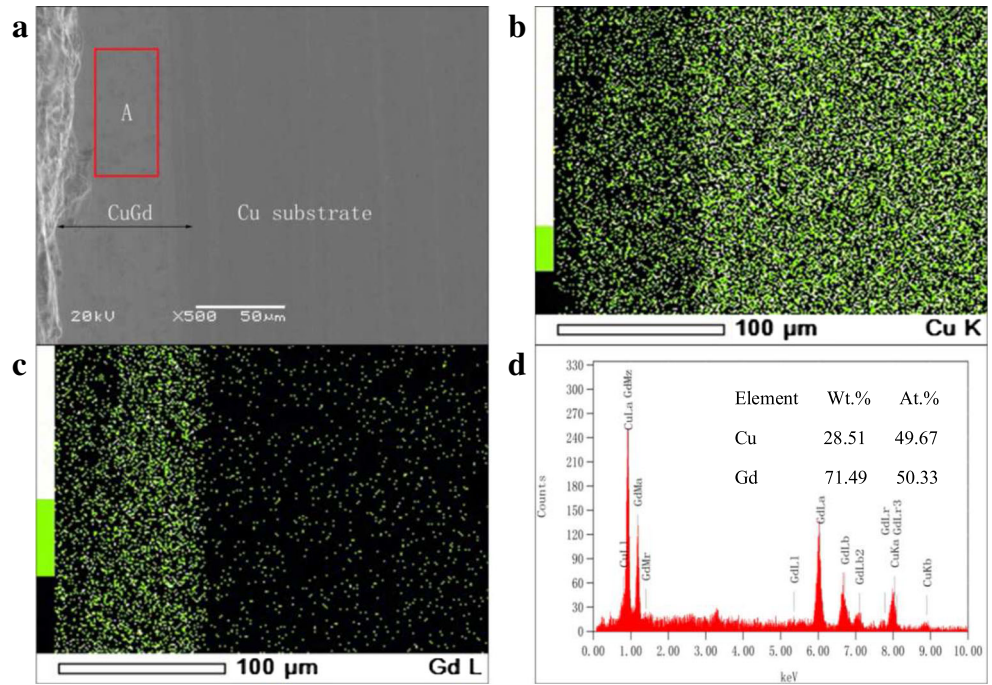


Fig. 13 SEM micrograph and EDS analysis of a cross section of Cu electrode in LiCl-KCl-GdCl₃ (1.48 wt.%) melts by potentiostatic electrolysis – 2.20 V for 12 h. Temperature: 823 K

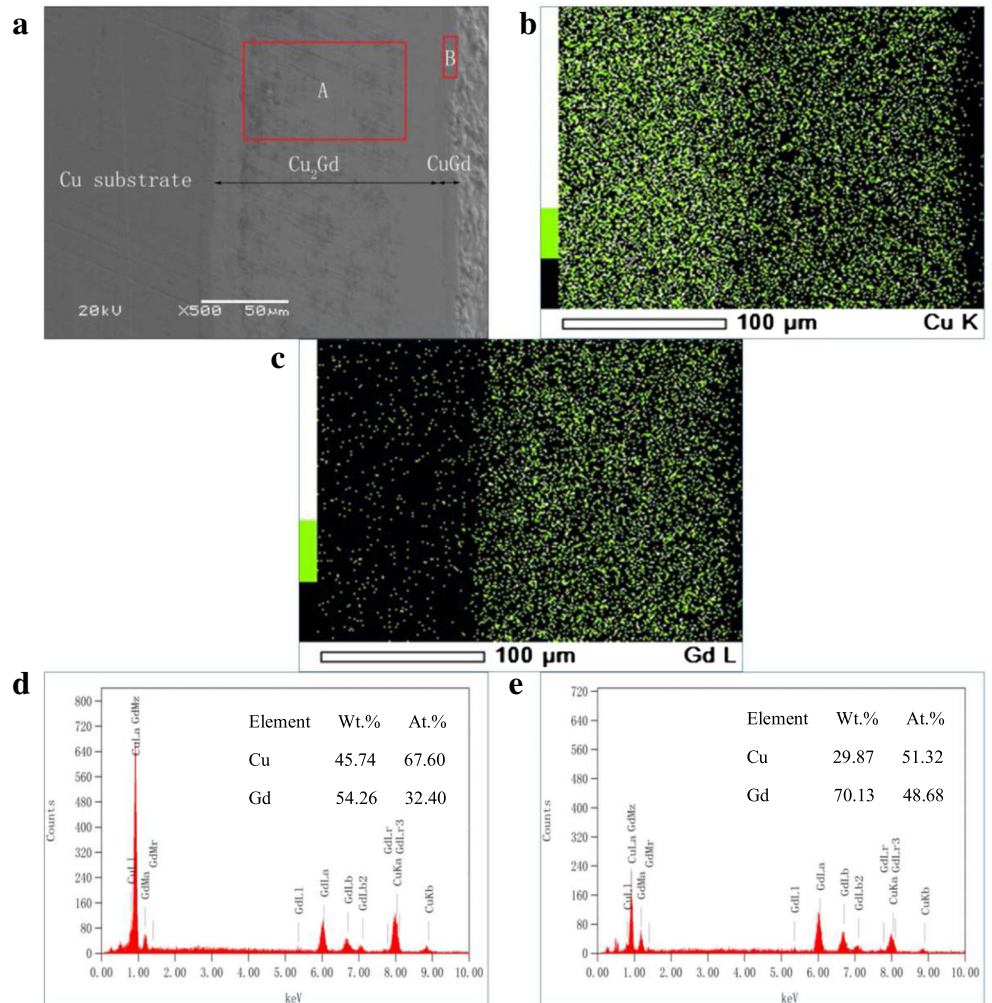


Fig. 14 SEM micrograph and EDS analysis of a cross section of Cu electrode in LiCl-KCl-GdCl₃ (1.48 wt.%) melts by potentiostatic electrolysis – 1.75 V for 10 h. Temperature: 823 K

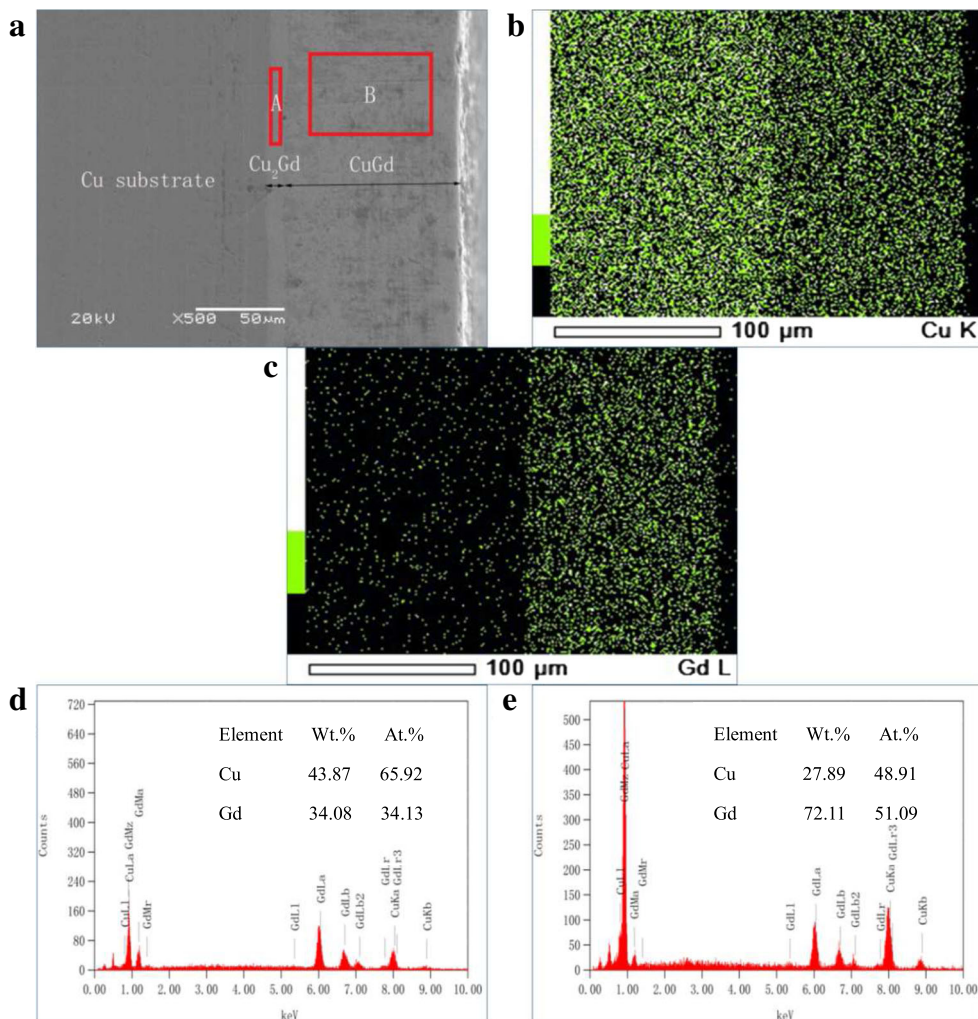
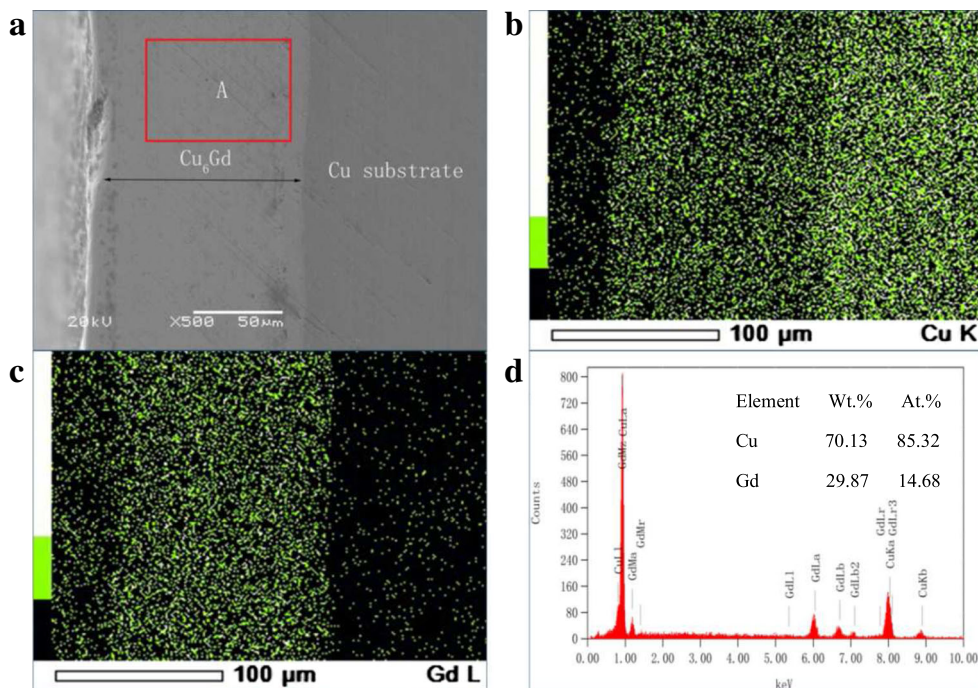


Fig. 15 SEM micrograph and EDS analysis of a cross section of Cu electrode in LiCl-KCl-GdCl₃ (1.48 wt.%) melts by potentiostatic electrolysis – 1.65 V for 10 h. Temperature: 823 K



99.60% after potentiostatic electrolysis at -2.20 V for 12 h in LiCl-KCl-GdCl₃ melts on Cu electrode. Kui Liu et al. [53] studied the co-reduction of Gd(III) ions and Al(III) ions, and the extraction efficiencies were 89.7% (potentiostatic electrolysis) and 96.5% (galvanostatic electrolysis), respectively. Compared with co-reduction on Mo electrode, the extraction of Gd on Cu electrode has higher extraction efficiency in the LiCl-KCl-GdCl₃ melts. Therefore, the extraction of Cu electrode is a good choice.

Figure 14 exhibited SEM micrograph and EDS analysis of a cross section of Cu electrode in LiCl-KCl-GdCl₃ (1.48 wt.%) melts by potentiostatic electrolysis electrolysis -1.64 V for 10 h at 823 K. From the SEM image (Fig. 14a), the thickness of the Cu-Gd alloy layer prepared is about 125 μm . The EDS results of the alloy layers (red frame A and B) taken from Fig. 14a indicates that the layers are composed of Cu and Gd, with Cu/Gd atomic ratios of about 65.92/34.08 (1.93/1) and 48.91/51.09 (0.96/1), respectively. Therefore, the alloy layers of the sample are composed of Cu₂Gd and CuGd, respectively, when the measurement error is taken into account. Figure 15 exhibited SEM micrograph and EDS analysis of a cross section of Cu electrode in LiCl-KCl-GdCl₃ (1.48 wt.%) melts by g potentiostatic electrolysis electrolysis -1.55 V for 10 h at 823 K. According to the potential curve, only a Cu-Gd intermetallic compound exist at more positive than -1.55 V. The thickness of the deposited alloy layer is about 120 μm , and Cu/Gd atomic ratios of about 85.32/14.68 (5.81/1). Therefore, the coating is composed of Cu₆Gd phase. According to the analysis results of XRD and SEM/EDS, Three intermetallic compounds I, II, and III are respectively CuGd, Cu₂Gd, and Cu₆Gd, respectively.

Conclusion

The electrochemical co-reduction of Gd(III) and Cu(II) was investigated, meanwhile the electrochemical behaviors of GdCl₃ in LiCl-KCl melts were first studied on W electrode. Cyclic voltammogram and square wave voltammogram indicated the reduction of Gd(III) ions in LiCl-KCl melts is a one-step three-electrons transfer process: $\text{Gd(III)} + 3e^- = \text{Gd(0)}$.

The equilibrium potential of Gd(III) was measured by open circuit potential curve in the temperature range of 773–893 K. The apparent standard potential, $E_{\text{Gd(III)/Gd(0)}}^{*0}$, and the apparent Gibbs free energy of formation for GdCl₃, $G_f^{*0}(\text{GdCl}_3)$ were calculated by experimental data.

The experiments of co-reduction of Gd(III) and Cu(II) on W electrode showed that three groups of peaks, corresponding to the formation of Gd_xCu_y intermetallic compounds, were detected from cyclic voltammogram, square wave voltammogram, and open circuit chronopotentiometry.

The electrochemical behavior of Gd(III) was explored on Cu electrode, and the reduction potentials of Gd(III)/Gd(0) on Cu electrode were observed at more positive than that on W electrode, by reason of the formation of Cu-Gd intermetallics. Galvanostatic/potentiostatic electrolysis was carried out to form Cu-Gd intermetallics characterized by XRD and SEM/EDS. The extraction efficiency was calculated during potentiostatic electrolysis at -2.20 V for 12 h at 823 K. According to the analysis results of XRD and SEM/EDS, three intermetallic compounds (CuGd, Cu₂Gd, and Cu₆Gd) were detected. It was found that the highest extraction efficiency could reach 99.60%. Therefore, the cycle of spent fuel by electrochemical extraction of Gd (fission products) proves to be satisfactory using Cu as working electrode.

Funding information The work was financially supported by the National Natural Science Foundation of China (11575047, 11675044, 21790373, 21271054, and 21173060), the Major Research Plan of the National Natural Science Foundation of China (91326113 and 91226201), National Natural Science Foundation of China (U1630102), and the Fundamental Research Funds for the Central Universities (HEUCFP201849).

References

- Salvatore M (2005) Nuclear fuel cycle strategies including partitioning and transmutation. Nucl Eng Des 235:805–816. <https://doi.org/10.1016/j.nucengdes.2004.10.009>
- Redkin A, Zaikov Y, Tkacheva O, Kumkov S (2016) Molar thermal conductivity of molten salts. Ionics 22:143–149. <https://doi.org/10.1007/s11581-015-1592-y>
- Chandrasekaran S, Basu P, Krishnan H, Sivasubramanian K, Baskaran R, Venkatraman B (2018) Development of gadolinium (neutron poison) monitoring system for fuel reprocessing facilities: computational model and validation with experiments. Prog Nucl Energ 107:57–60. <https://doi.org/10.1016/j.pnucene.2018.04.004>
- Liu K, Liu YL, Pang JW, Yuan LY, Wang L, Chai ZF, Shi WQ (2017) Condition dependence of Zr electrochemical reactions and morphological evolution of Zr deposits in molten salt. Sci China Chem 60(2):1–11. <https://doi.org/10.1007/s11426-016-0321-x>
- Iida T, Nohira T, Ito Y (2003) Electrochemical formation of Sm-Co alloys by codeposition of Sm and Co in a molten LiCl-KCl-SmCl₃-CoCl₂ system. Electrochim Acta 48(17):2517–2521. [https://doi.org/10.1016/S0013-4686\(03\)00293-7](https://doi.org/10.1016/S0013-4686(03)00293-7)
- Yan YD, Tang H, Zhang ML, Xue Y, Han W, Cao DX, Zhang ZJ (2012) Extraction of europium and electrodeposition of Al-Li-Eu alloy from Eu₂O₃ assisted by AlCl₃ in LiCl-KCl melt. Electrochim Acta 59:531–537. <https://doi.org/10.1016/j.electacta.2011.11.007>
- Gibilaro M, Massot L, Chamelot P, Taxil P (2009) Co-reduction of aluminium and lanthanide ions in molten fluorides: application to cerium and samarium extraction from nuclear wastes. Electrochim Acta 54:5300–5306. <https://doi.org/10.1016/j.electacta.2009.01.074>
- Gibilaro M, Massot L, Chamelot P, Taxil P (2008) Study of neodymium extraction in molten fluorides by electrochemical reduction with aluminium. J Nucl Mater 382:39–45. <https://doi.org/10.1016/j.jnucmat.2008.09.004>
- Ping XY, Liu K, Liu YL, Yuan LY, Yao BL, Zhao XL, Chai ZF, Shi WQ (2017) Direct electrochemical preparation of Ni-Zr alloy from

- mixture oxides in LiCl molten salt. *J Electrochem Soc* 164(13): D888–D894. <https://doi.org/10.1149/2.1361713jes>
10. Pang JW, Liu K, Liu YL, Nie CM, Luo LX, Yuan LY, Chai ZF, Shi WQ (2016) Electrochemical properties of lanthanum on the liquid gallium electrode in LiCl-KCl eutectic. *J Electrochem Soc* 163(14): D750–D756. <https://doi.org/10.1149/2.0611614jes>
 11. Zhou W, Liu YL, Liu K, Liu ZR, Yuan LY, Wang L, Feng YX, Chai ZF, Shi WQ (2015) Electroreduction of Gd³⁺ on W and Zn electrodes in LiCl-KCl eutectic: a comparison study. *J Electrochem Soc* 162(10):D531–D539. <https://doi.org/10.1149/2.0541510jes>
 12. Wang L, Liu YL, Liu K, Tang SL, Yuan LY, Lu T, Chai ZF, Shi WQ (2015) Electrochemical extraction of cerium by forming Ce-Zn alloys in LiCl-KCl eutectic on W and liquid Zn electrodes. *J Electrochem Soc* 162(9):E179–E184. <https://doi.org/10.1149/2.1141509jes>
 13. Liu YL, Liu K, Yuan LY, Chai ZF, Shi WQ (2016) Estimation of the intermetallic compounds in LiCl-KCl molten salt by cyclic voltammetry. *Faraday Discuss* 190:387–398. <https://doi.org/10.1039/c5fd00220f>
 14. Castrillejo Y, Bermejo MR, Díaz Arocas P, Martínez AM, Barrado E (2005) Electrochemical behaviour of praseodymium (III) in molten chlorides. *J Electroanal Chem* 575:61–74. <https://doi.org/10.1016/j.jelechem.2004.08.020>
 15. Castrillejo Y, Bermejo MR, Barrado AI, Pardo R, Barrado E, Martínez AM (2005) Electrochemical behaviour of dysprosium in the eutectic LiCl-KCl at W and Al electrodes. *Electrochim Acta* 50: 2047–2057. <https://doi.org/10.1016/j.electacta.2004.09.013>
 16. Bermejo MR, Gómez J, Medina J, Martínez AM, Castrillejo Y (2006) The electrochemistry of gadolinium in the eutectic LiCl-KCl on W and Al electrodes. *J Electroanal Chem* 588:253–266. <https://doi.org/10.1016/j.jelechem.2005.12.031>
 17. Castrillejo Y, Bermejo MR, Barrado E, Martínez AM (2006) Electrochemical behaviour of erbium in the eutectic LiCl-KCl at W and Al electrodes. *Electrochim Acta* 51:1941–1951. <https://doi.org/10.1016/j.electacta.2005.07.004>
 18. Castrillejo Y, Bermejo MR, Barrado E, Medina J, Martínez AM (2006) Electrodeposition of Ho and electrochemical formation of Ho-Al alloys from the eutectic LiCl-KCl. *J Electrochem Soc* 153: C713–C721. <https://doi.org/10.1149/1.2257971>
 19. Bermejo MR, de la Rosa F, Barrado E, Castrillejo Y (2007) Cathodic behaviour of europium (III) on glassy carbon, electrochemical formation of Al₄Eu, and oxoacidity reactions in the eutectic LiCl-KCl. *J Electroanal Chem* 603:81–95. <https://doi.org/10.1016/j.jelechem.2007.01.018>
 20. Bermejo MR, Barrado E, Martínez AM, Castrillejo Y (2008) Electrodeposition of Lu on W and Al electrodes: electrochemical formation of Lu-Al alloys and oxoacidity reactions of Lu(III) in the eutectic LiCl-KCl. *J Electroanal Chem* 617:85–100. <https://doi.org/10.1016/j.jelechem.2008.01.017>
 21. Castrillejo Y, Fernández P, Bermejo MR, Barrado E, Martínez AM (2009) Electrochemistry of thulium on inert electrodes and electrochemical formation of a Tm-Al alloy from molten chlorides. *Electrochim Acta* 54:6212–6222. <https://doi.org/10.1016/j.electacta.2009.05.095>
 22. Castrillejo Y, Fernández P, Medina J, Vega M, Barrado E (2011) Chemical and electrochemical extraction of ytterbium from molten chlorides in pyrochemical processes. *Electroanal* 23:222–236. <https://doi.org/10.1002/elan.201000421>
 23. Castrillejo Y, Fernández P, Medina J, Hernández P, Barrado E (2011) Electrochemical extraction of samarium from molten chlorides in pyrochemical processes. *Electrochim Acta* 56:8638–8644. <https://doi.org/10.1016/j.electacta.2011.07.059>
 24. Li M, Gu QQ, Han W, Yan YD, Zhang ML, Sun Y, Shi WQ (2015) Electrodeposition of Tb on Mo and Al electrodes: thermodynamic properties of TbCl₃ and TbAl₂ in the LiCl-KCl eutectic melts. *Electrochim Acta* 167:139–146. <https://doi.org/10.1016/j.electacta.2015.03.145>
 25. Cassayre L, Malmbeck R, Massot P, Rebizant J, Serp J, Soucek P, Glatz JP (2007) Investigation of electrorefining of metallic alloy fuel onto solid Al cathodes. *J Nucl Mater* 360:49–57. <https://doi.org/10.1016/j.jnucmat.2006.08.013>
 26. Taxil P, Massot L, Nourry C, Gibilaro M, Chamelot P, Cassayre L (2009) Lanthanides extraction processes in molten fluoride media: application to nuclear spent fuel reprocessing. *J Fluor Chem* 130: 94–101. <https://doi.org/10.1016/j.jfluchem.2008.07.004>
 27. Gibilaro M, Massot L, Chamelot P, Cassayre L, Taxil P (2009) Electrochemical extraction of europium from molten fluoride media. *Electrochim Acta* 55:281–287. <https://doi.org/10.1016/j.electacta.2009.08.052>
 28. Nourry C, Massot L, Chamelot P, Taxil P (2009) Neodymium and gadolinium extraction from molten fluorides by reduction on a reactive electrode. *J Appl Electrochem* 39:2359–2367. <https://doi.org/10.1007/s10800-009-9922-2>
 29. Nourry C, Massot L, Chamelot P, Taxil P (2009) Electrochemical reduction of Gd(III) and Nd(III) on reactive cathode material in molten fluoride media. *J Appl Electrochem* 39:927–933. <https://doi.org/10.1007/s10800-008-9740-y>
 30. Saïla A, Gibilaro M, Massot L, Chamelot P, Taxil P, Affoune AM (2010) Electrochemical behaviour of dysprosium(III) in LiF-CaF₂ on Mo, Ni and Cu electrodes. *J Electroanal Chem* 642:150–156. <https://doi.org/10.1016/j.jelechem.2010.03.002>
 31. Wang YC, Li M, Han W, Zhang ML, Jiang T, Peng SM, Yan YD (2017) Electrochemical behaviour of erbium(III) and its extraction on Cu electrode in LiCl-KCl melts. *J Alloys Compd* 695:3484–3494. <https://doi.org/10.1016/j.jallcom.2016.12.008>
 32. Li M, Liu B, Ji N, Sun Y, Han W, Jiang T, Peng SM, Yan YD, Zhang ML (2016) Electrochemical extracting variable valence ytterbium from LiCl-KCl-YbCl₃ melt on Cu electrode. *Electrochim Acta* 193:54–62. <https://doi.org/10.1016/j.electacta.2016.02.020>
 33. Han W, Li ZY, Li M, Hu X, Yang XG, Zhang ML, Sun Y (2017) Electrochemical behavior and extraction of holmium on Cu electrode in LiCl-KCl molten salt. *J Electrochem Soc* 164(13):D934–D943. <https://doi.org/10.1149/2.0101714jes>
 34. Yasuda K, Kondo K, Nohira T, Hagiwara R (2014) Electrochemical formation of Pr-Ni alloys in LiF-CaF₂-PrF₃ and NaCl-KCl-PrCl₃ melts. *J Electrochem Soc* 161(7):D3097–D3104. <https://doi.org/10.1149/2.012407jes>
 35. Yasuda K, Kobayashi S, Nohira T, Hagiwara R (2013) Electrochemical formation of Dy-Ni alloys in molten NaCl-KCl-DyCl₃. *Electrochim Acta* 106:293–300. <https://doi.org/10.1016/j.electacta.2013.05.095>
 36. Yasuda K, Kobayashi S, Nohira T, Hagiwara R (2013) Electrochemical formation of Nd-Ni alloys in molten NaCl-KCl-NdCl₃. *Electrochim Acta* 92:349–355. <https://doi.org/10.1016/j.electacta.2013.01.049>
 37. Han W, Sheng QN, Zhang ML, Li M, Sun TT, Liu YC, Ye K, Yan YD, Wang YC (2014) The electrochemical formation of Ni-Tb intermetallic compounds on a nickel electrode in the LiCl-KCl eutectic melts. *Metall Mater Trans B Process Metall Mater Process Sci* 45:929–935. <https://doi.org/10.1007/s11663-013-9984-8>
 38. Konishia H, Mizumaa K, Onoa H, Takeuchia E, Nohirab T, Oishic T (2012) Electrochemical formation of Tb-Ni alloys in a molten LiCl-KCl-TbCl₃ system. *ECS Trans* 50(11):561–569. <https://doi.org/10.1149/05011.0561ecst>
 39. Iida T, Nohira T, Ito Y (2003) Electrochemical formation of Yb/Ni alloy films by Li codeposition method in a molten LiCl-KCl-YbCl₃ system. *Electrochim Acta* 48:1531–1536. [https://doi.org/10.1016/S0013-4686\(03\)00031-8](https://doi.org/10.1016/S0013-4686(03)00031-8)
 40. Iida T, Nohira T, Ito Y (2001) Electrochemical formation of Sm-Ni alloy films in a molten LiCl-KCl-SmCl₃ system. *Electrochim Acta* 46:2537–2544. [https://doi.org/10.1016/S0013-4686\(01\)00470-4](https://doi.org/10.1016/S0013-4686(01)00470-4)

41. Yang YS, Zhang ML, Han W, Sun PY, Liu B, Jiang HL, Jiang T, Peng SM, Li M, Ye K, Yan YD (2014) Selective electrodeposition of dysprosium in LiCl-KCl-GdCl₃-DyCl₃ melts at magnesium electrodes: application to separation of nuclear wastes. *Electrochim Acta* 118:150–156. <https://doi.org/10.1016/j.electacta.2013.11.145>
42. Wang YC, Li M, Han W, Zhang ML, Yang YS, Sun Y, Zhao YC, Yan YD (2015) Electrochemical extraction and separation of praseodymium and erbium on reactive magnesium electrode in molten salts. *J Solid State Elect* 19:3629–3638. <https://doi.org/10.1007/s10008-015-2989-2>
43. Nicholson RS, Shain I (1964) Theory of stationary electrode polarography. Single scan and cyclic methods applied to reversible, irreversible, and kinetic systems. *Anal Chem* 36(4):706–723. <https://doi.org/10.1021/ac60210a007>
44. Tang H, Pesic B (2014) Electrochemical behavior of LaCl₃ and morphology of La deposit on molybdenum substrate in molten LiCl-KCl eutectic salt. *Electrochim Acta* 119:120–130. <https://doi.org/10.1063/1.3575107>
45. Bard AJ, Faulkner LR (2001) *Electrochemical methods: fundamentals and applications*. Wiley, New York
46. Ramaley L, Krasue MS Jr (1969) Theory of square wave voltammetry. *Anal Chem* 41:1362–1365. <https://doi.org/10.1021/ac60280a005>
47. Osteryoung JG, Osteryoung RA (1985) Square wave voltammetry. *Anal Chem* 57(1):101A–110A. <https://doi.org/10.1021/ac00279a789>
48. Castrillejo Y, Bermejo MR, Barrado E, Martinez A, Diaz Arocas P (2003) Solubilization of rare earth oxides in the eutectic LiCl-KCl mixture at 450°C and in the equimolar CaCl₂-NaCl melt at 550°C. *J Electroanal Chem* 545:141–157. [https://doi.org/10.1016/S0022-0728\(03\)00092-5](https://doi.org/10.1016/S0022-0728(03)00092-5)
49. Fusselman SP, Roy JJ, Grimmer DL, Grantham LF, Krueger CL, Nabelek CR, Storvick TS, Inoue T, Hijikata T, Kinoshita K, Sakamura Y, Uozumi K, Kawai T, Takahashi N (1999) Thermodynamic properties for rare earths and americium in pyropartitioning process solvents. *J Electrochem Soc* 146:2573–2580. <https://doi.org/10.1149/1.1391974>
50. Bagri P, Simpson MF (2018) Potentiometric measurement of activity of rare earth chlorides (La, Gd, Ce, Nd) in LiCl-KCl eutectic salt. *Electrochim Acta* 259:1120–1128. <https://doi.org/10.1016/j.electacta.2017.10.082>
51. Zhou WT, Wang YF, Zhang JS, Khafizov M (2018) Calculated thermodynamic properties of GdCl₃ in LiCl-KCl eutectic molten salt. *J Nucl Mater* 508:40–50. <https://doi.org/10.1016/j.jnucmat.2018.05.030>
52. Castrillejo Y, Abejón C, Vega M, Pardo R, Barrado E (1997) Chemical and electrochemical behaviour of copper ions in the ZnCl₂-2NaCl mixture at 450°C. *Electrochim Acta* 40(17):2731–2738. [https://doi.org/10.1016/0013-4686\(95\)00256-E](https://doi.org/10.1016/0013-4686(95)00256-E)
53. Liu K, Liu YL, Yuan LY, Zhao XL, Chai ZF, Shi WQ (2013) Electroextraction of gadolinium from Gd₂O₃ in LiCl-KCl-AlCl₃ molten salts. *Electrochim Acta* 109:732–740. <https://doi.org/10.1016/j.electacta.2013.07.084>